Heterogeneous catalysis

DOI: 10.1002/anie.200((will be filled in by the editorial staff))

Local light-off in catalytic CO oxidation on low-index Pt and Pd surfaces: a combined PEEM, MS and DFT study**

*Diana Vogel, Christian Spiel, Yuri Suchorski, Adriana Trinchero, Robert Schlögl, Henrik Grönbeck, Günther Rupprechter**

Although modern catalytic converters significantly reduce pollution from automobile engines, a major amount of pollutants is still emitted just after "cold-start", i.e. until the catalytic converter warms up to its "ignition" temperature, at which the reaction rate rapidly switches from low to high conversion. There is thus substantial interest of manufacturers to reduce emissions during the start-up period of automotive catalysts. Consequently, sophisticated catalyst heating processes have been developed to quickly reach the critical temperature. Methods include operation at lean air-to-fuel ratio, exhaust system combustion devices, secondary air injection into the exhaust, electrically heated catalysts, etc.[1] Alternatively, as an "energy-neutral" approach, lowering the critical temperature seems more promising.

Catalytic ignition has originally been considered as a sole heat balance problem,[2] with the critical ignition temperature being defined as the temperature when the heat generated by the exothermic reaction exceeds the dissipated heat (i.e. the catalyst heats up and no external heating is required anymore; "light-off"). In fact, the catalytic ignition process represents a convolution of reaction kinetics and heat generation, since the produced heat is governed by the reaction rate which in turn is determined by the reaction kinetics.[3,4]

However, for CO oxidation under (ultra)high-vacuum on model catalysts, the heat generation by the reaction can be neglected, and the catalytic ignition problem can thus be reduced to the "pure kinetics", i.e. to the temperature-triggered kinetic transition from the low-rate steady state regime to a high-rate steady state.[5,6] Such a transition in the CO oxidation reaction is a phenomenon of pure kinetic origin[7,8] which is well studied, mainly via varying the CO/O_2 ratio.[9-12]

In this work we present an experimental and theoretical study of catalytic ignition in the CO oxidation reaction under high vacuum conditions (10^{-5} mbar range), for μm-sized (hkl) domains of polycrystalline Pt and Pd foil. Emphasis is put on local kinetic measurements enabling a direct comparison of the reaction properties of low-Miller-index Pt(hkl) and Pd(hkl) domains. To our knowledge this is the first time that the different metals and different terminations have been evaluated under basically identical reaction conditions, yielding the inherent reaction behavior. It is demonstrated that the isothermal and the isobaric determination of reactivity states yield equivalent results in the considered pressure regime for the CO oxidation on Pt and Pd foil. Regarding the reactivity range in (p, T)-parameter space, Pd foil is the better-suited catalyst for CO oxidation than Pt foil since Pd is poisoned and also reactivated at higher CO-to-oxygen pressure ratios (i.e. Pd is more CO-tolerant). These experimental findings are supported and explained by Density Functional Theory (DFT) calculations.

Recently, we have developed an experimental approach, based on the analysis of local PEEM (Photoemission Electron Microscopy) intensities, which allows the in situ observation of kinetic phase transitions on individual differently oriented grains of a polycrystalline Pt foil.[12] The idea of the experiment is based on the fact that the local photoemission yield is directly dependent on the local CO or oxygen coverage (via the local work function). Since the CO or oxygen coverage governs the rate of CO_2 formation,[13] the local PEEM image intensity serves as an indicator for the local reaction rate, which allows "imaging" of the kinetic phase transitions on the μm-scale. Previously, we have used such an analysis to construct kinetic phase diagrams for the CO oxidation reaction in the 10^{-5} mbar pressure range for individual [100]-, [110]- and [111]-oriented grains of a Pt foil.[12] The single (hkl) domains exhibited independent reaction properties, analogous to the corresponding single crystals, and the sum of the local kinetic diagrams for individual grains is equal to the global kinetic diagram obtained for the whole sample by MS (indicating that the grain boundaries do not contribute directly to the overall reactivity and that all relevant catalytic processes were monitored by this approach).[12] In the present contribution, this approach has been extended to Pd samples and to the reaction light-off on Pt and Pd foil at isobaric conditions.

[*] D. Vogel, Dr. C. Spiel, Assoc. Prof. Dr. Y. Suchorski, Prof. Dr. G. Rupprechter
Institute of Materials Chemistry
Vienna University of Technology
Getreidemarkt 9/BC/01, A-1060 Vienna, Austria
Fax: (+) 43-1-58801-16599
E-mail: grupp@imc.tuwien.ac.at
Homepage: www.imc.tuwien.ac.at

A. Trinchero, Prof. Dr. H. Grönbeck
Department of Applied Physics and Competence Centre for Catalysis
Chalmers University of Technology
SE-41296 Göteborg, Sweden

D. Vogel, Prof. Dr. R. Schlögl
Department of Inorganic Chemistry
Fritz-Haber-Institute of the Max-Planck-Society
Faradayweg 4-6, D-14195 Berlin, Germany.

[**] This work was supported by the Austrian Science Fund (FWF) [SFB-F45-04 FOXSI]. Technical support by Johannes Frank (IMC, TU Vienna) is cordially acknowledged.

Supporting information for this article is available on the WWW under http://www.angewandte.org or from the author.

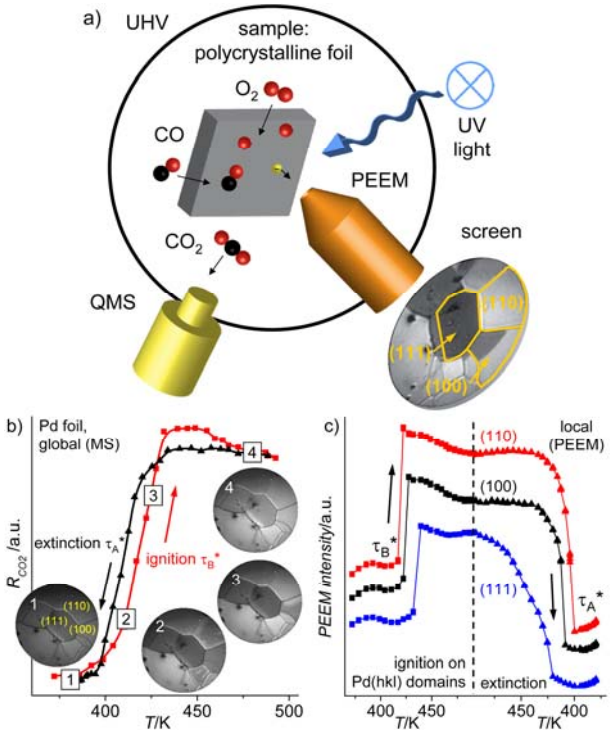

Figure 1. a) Scheme of the experiment: CO oxidation reaction on polycrystalline Pd (Pt) foil is simultaneously followed by MS and PEEM. Three different domains, Pd(110), Pd(100) and Pd(111) are exemplary identified in the PEEM image. b) Ignition (red squares) and extinction curves (black triangles) on Pd foil, as CO_2 production rate measured globally by MS at cyclic variation of the sample temperature (rate: 0.5 K/s) at constant p_{CO} = 5.8x10^{-6} mbar and p_{O2} = 1.3x10^{-5} mbar. Simultaneously recorded PEEM video-sequences illustrate the ignition process: Frame (1) - inactive, CO covered surface; (2) - ignition begins on (110)-domains; (3) - ignition continues on (100) domains; (4) - oxygen covered, active surface. c) Laterally resolved ignition/extinction measurements: local PEEM intensity for the individual (110), (100) and (111) domains during the same cyclic temperature scan as in (b). The vertical dashed line indicates the turning point from heating to cooling.

A series of ignition/extinction experiments has been performed in a UHV chamber with a base pressure <10^{-9} mbar on polycrystalline Pd (AlfaAesar, 99.9%) and Pt (MaTecK, 99.99%) foil, both consisting of up to ~100 µm large crystallites of different surface orientation, as determined by work function analysis.[12] The reaction was followed in situ (Figure 1a), simultaneously by photoemission electron microscopy (PEEM) and by quadrupole mass spectrometry (QMS). QMS provides the average CO_2 formation rate originating from all grains of the polycrystalline foil (Figure 1b), whereas the recorded PEEM-sequences deliver the local photoemission yield from individual grains (Figure 1c). The latter provides laterally-resolved kinetic information from the different domains at exactly identical experimental conditions, since all domains of the foil are exposed to the same gas phase composition at the same temperature. In this way, the global (Figure 1b) and local (Figure 1c) kinetics for the Pd foil can be compared, e.g. for a typical temperature scan from 372 K to 493 K, with a rate of 0.5 K/s at constant p_{CO} = 5.8x10^{-6} mbar and p_{O2} = 1.3x10^{-5} mbar. Following the temperature ramp, the global CO_2 rate suddenly increases indicating the transition τ_B^* from the state of low catalytic activity (CO-poisoned surface; video-frame 1 in Figure 1b, dark contrast) to the state of high catalytic activity at which the surface becomes oxygen covered (frame 4; bright contrast). Analogous to the MS signal in the overall CO_2 reaction rate, the jumps in the local PEEM intensity represent the local kinetic transitions on the individual grains (Figure 1c). These transitions do not occur simultaneously on the different orientations but show a pronounced structure sensitivity with clearly identifiable critical temperatures of 417 K for Pd(110), 423 K for Pd(100) and 432 K for Pd(111). A similar observation was made for the reaction extinction, i.e. for the transition τ_A^* from the high reactivity to the low reactivity state upon cooling the sample. Again, the curve of the *global* CO_2 production rate appears to be "smoothened out" (black curve in Figure 1b), whereas *local* extinction on the individual grains occurs rather sharply and independently from each other (Figure 1c). This clearly shows the limitation of averaging techniques such as mass-spectroscopy, which can not reveal the important local kinetics.

Usually, kinetic transitions in CO oxidation were experimentally studied under high vacuum conditions by varying the CO/O_2 pressure ratio at constant temperature.[9,10,12] Such an experiment is illustrated for Pd foil in the right inset of Figure 2a, at constant p_{O2} = 1.3x10^{-5} mbar and T = 449 K. Similar to the case of Pt foil,[12,14,15] the global CO_2 formation rate exhibits a pronounced hysteresis upon cyclic variation of the CO partial pressure manifested in the gap between the kinetic transition τ_A from the high reactivity to the low reactivity state and the reverse transition τ_B. In between, the system is bistable, i.e. it can be either in the high or in the low reactivity steady state, depending on the prehistory. The τ_A and τ_B points are temperature-dependent, thus a (global) kinetic phase diagram can be constructed for the Pd foil, summarizing the kinetic transitions (Figure 2a).

For comparison, the kinetic transition points (τ_A^*/τ_B^*) extracted from isobaric ignition/extinction experiments (shown in the left inset of Figure 2a for constant p_{CO} = 5.8x10^{-6} mbar and p_{O2} = 1.3x10^{-5} mbar) are also plotted into the isothermally obtained diagram in Figure 2a. The *isobaric* variation of the reaction temperature results in kinetic transitions which are quantitatively matching the kinetic phase diagram obtained by the *isothermal* variation of the CO pressure. In Figure 2b the result of the local PEEM analysis of the same transition for an individual Pd(100) domain is shown: again, the left inset shows the ignition/extinction experiment and the right inset presents the transitions obtained via variation of the CO pressure at constant T and p_{O2}. As in the case of the (global) MS-data, the transition points obtained from isobaric experiments are in quantitative agreement with the isothermal experiments, thus linking the typical surface science (isothermal) approach and the typical technical catalysis (isobaric) approach.

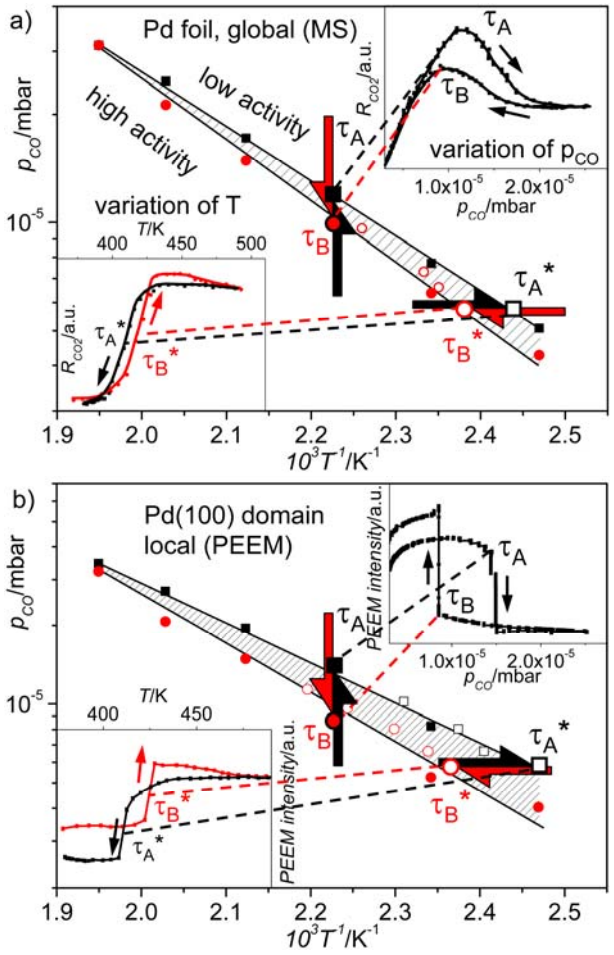

Figure 2. Global (a) and local (b) kinetic phase diagram illustrating the CO oxidation reaction on polycrystalline Pd foil (a) and on a single Pd(100) domain of the Pd foil (b). Note the agreement of the transition points τ_A* and τ_B* obtained at varying T (from the ignition/extinction curves shown in the left insets) with the diagram obtained via cyclic variation of p_{CO} (from the poisoning/reactivation curves in the right insets). The dashed regions indicate the range of bistability.

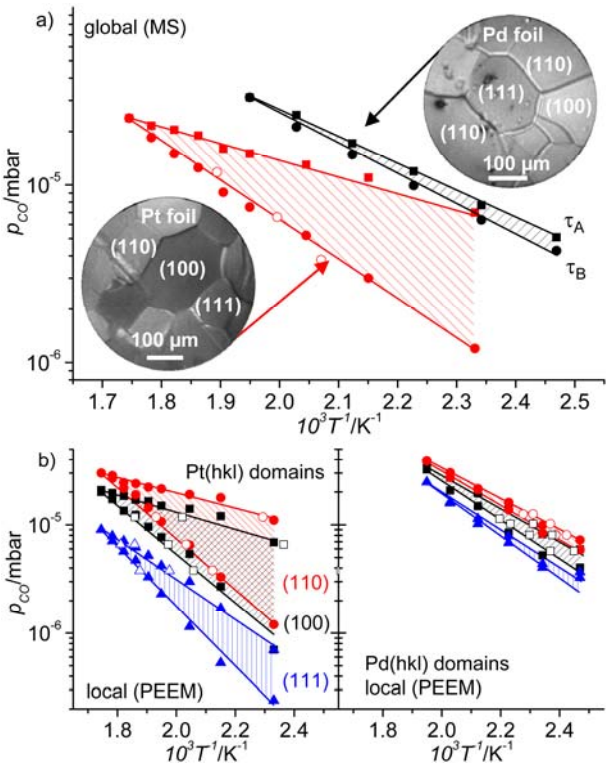

Figure 3. Palladium versus platinum in CO oxidation. a) Comparison of the global kinetic phase diagrams (by MS) at constant oxygen pressure (p_{O2} = 1.3x10^{-5} mbar) of polycrystalline Pt (filled red squares and circles) and Pd (black squares and circles)[1]. Open circles are ignition points for Pt. b) Corresponding local kinetic phase diagrams for individual Pt(hkl) domains (left) and Pd (right), obtained by local PEEM intensity analysis. Open symbols are the local ignition and extinction points.

In Figure 3a, the *global* reaction behavior of Pt and Pd foil is compared, whereas in Figure 3b the *local* kinetic transitions of the individual Pt(hkl) domains are contrasted to those of the Pd(hkl) domains. The most striking differences between Pt and Pd are: (i) the global and the respective local kinetic phase diagrams of Pd foil are situated at significantly higher CO partial pressure and (ii) the bistability range is much narrower for Pd than for Pt foil. In particular, this means that for Pd the transition τ_A from the high to the low reactivity state occurs at higher CO partial pressure than for Pt, and that the reverse transition τ_B also occurs at a higher CO-to-oxygen ratio than for Pt. In other words, Pd is the better (more CO-tolerant) catalyst than Pt under the current conditions because *more* CO is needed to poison the Pd surface and a *lower* oxygen-to-CO ratio is sufficient to "reactivate" the Pd surface. Besides that, the bistability regime of Pd disappears at a lower temperature than in the case of Pt, namely at T_{Pd} = 513 K in contrast to T_{Pt} = 573 K, so already at lower temperature Pd cannot be poisoned by CO anymore.

In order to explain these observations, density functional theory (DFT) has been applied to calculate the adsorption energies of CO and oxygen on clean Pd(hkl) and Pt(hkl) domains, as well as the reaction barriers (cf. Table 1, supporting information). The sticking coefficients of CO and oxygen and the desorption temperatures of CO on Pd(hkl) and Pt(hkl), known from literature, are also included in Table 1. The bistability regions for Pt(111), Pt(100), Pt(110) and Pd(111) have been simulated by a micro-kinetic model (for details see supporting information) based on the conventional Langmuir-Hinshelwood mechanism. In Figure 4a the calculated bistability regions are compared for Pd(111) and Pt(111), and in Figure 4b the three low Miller-indexed surfaces of Pt are compared to each other. The right inset in Figure 4a depicts a simulated ignition/extinction curve for the Pd(111) surface, and the left inset shows a simulated hysteresis curve for the Pt(111) surface resulting from p_{CO} variation. In all cases, the kinetic simulations are in agreement with the experiment: the bistability region of Pd is considerably narrower than in case of Pt, and the kinetic phase diagram of Pd is located at higher CO pressure. The DFT-derived order of the local kinetic phase diagrams of the three Pt surfaces also corresponds to the experimental results: The Pt(100) surface is active at higher CO pressures than Pt(111), and Pt(110) is active at the highest CO pressures.

[1]An improved temperature measurement method was used in comparison to Ref. [12], with the corresponding correction being applied to the Pt data.

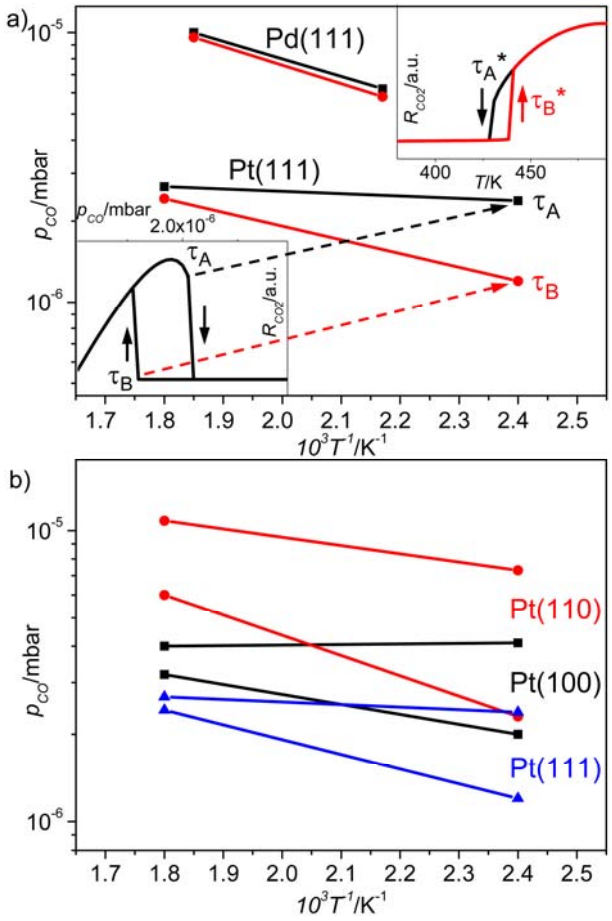

Figure 4. a) Simulated kinetic phase diagrams for Pd(111) and Pt(111) at p_{O2} = 1.3x10^{-5} mbar, as well as a simulated p_{CO} hysteresis curve for Pt(111) at 417 K (left inset) and a simulated ignition/extinction curve for Pd(111) at p_{CO} = 5.8x10^{-6} mbar (right inset). b) Simulated local kinetic phase diagrams of Pt(110), Pt(100) and Pt(111) at p_{O2} = 1.3x10^{-5} mbar.

The DFT calculations and the kinetic modelling provide an unambiguous way to rationalize the experimental findings. The experiments showed that at a given oxygen pressure and temperature the Pt(hkl) domains are deactivated at lower CO pressure than Pd(hkl). This can mainly be attributed to the higher adsorption energies of oxygen on Pd(hkl) than on Pt(hkl) (cf. Table 1, supporting information), i.e. oxygen is more strongly bound to Pd and thus, the CO-poisoning of the surface occurs at higher CO pressures. Regarding the transition τ_B from the low to the high reactivity state, the Pd foil "reactivates" already at a considerably higher CO pressure than Pt foil. This results from the higher sticking coefficients of oxygen for the Pd(hkl) domains as compared to the Pt(hkl) domains: whereas CO adsorption properties are quite similar on Pt and Pd(hkl) surfaces, oxygen adsorption is clearly favored on Pd(hkl). The disappearance of the bistability regime at the so-called "cusp-point" occurs at lower temperature for Pd than for Pt foil. This can be explained by the generally lower desorption temperature of CO on Pd(hkl).

In summary, local domain-specific kinetic measurements for individual Pd and Pt crystalline grains have been performed under truly identical reaction conditions, allowing a direct comparison of inherent catalytic properties of Pt(hkl)- and Pd(hkl)-domains with respect to CO oxidation. It has been shown that for the CO oxidation reaction the typical surface science approach for determining reaction kinetics, i.e. the isothermal monitoring of kinetic transitions, *quantitatively* yields the same results as the common technical catalysis approach, i.e. the isobaric study of the different reactivity regimes, at least in the pressure range of ~10^{-5} mbar. The observed differences in the catalytic activity of Pt(hkl)- and Pd(hkl)-domains, such as the much higher CO-tolerance and the higher reactivation ability of Pd as compared to Pt, as well as the differences between particular crystallographic orientations, were rationalized by DFT calculations and kinetic reaction modelling.

Received: ((will be filled in by the editorial staff))
Published online on ((will be filled in by the editorial staff))

Keywords: CO oxidation · heterogeneous catalysis · catalytic ignition · photoemission electron microscopy · density functional calculations

[1] C. Gong, K. Huang, B. Deng, X. Liu, *Energy* **2011**, *36*, 53-59.
[2] D. A. Frank-Kamenetskii, *Diffusion and heat transfer in chemical kinetics*, 2nd Ed., Plenum, New York, **1969**.
[3] M. Rinnemo, D. Kulginov, S. Johannson, K. L. Wong, V. P. Zhdanov, B. Kasemo, *Surf. Sci.* **1997**, *376*, 297-309.
[4] G. Eigenberger, *Chem. Eng. Sci.* **1978**, *33*, 1255-1261.
[5] M. Bowker, I. Z. Jones, R. A. Bennett, F. Esch, A. Baraldi, S. Lizzit, G. Comelli, *Catal. Lett.* **1998**, *51*, 187-190.
[6] R. A. Bennett, I. Z. Jones, M. Bowker, *Top. Catal.* **2007**, *42-43*, 373-376.
[7] V. P. Zhdanov, B. Kasemo, *Surf. Sci. Rep.* **1994**, *20*, 113-189.
[8] A. S. Mikhailov, *Foundations of Synergetics*, Springer, Berlin, **1990**.
[9] M. Ehsasi, M. Berdau, T. Rebitzki, K.-P. Charlé, J. H. Block, *J. Chem. Phys.* **1993**, *98*, 9177-9184.
[10] M. Berdau, G. G. Yelenin, A. Karpowicz, M. Ehsasi, K. Christmann, J. H. Block, *J. Chem. Phys.* **1999**, *110*, 11551-11573.
[11] Y. Suchorski, R. Wrobel, S. Becker, H. Weiss, *J. Phys. Chem. C* **2008**, *112*, 20012-20017.
[12] Y. Suchorski, C. Spiel, D. Vogel, W. Drachsel, R. Schlögl, G. Rupprechter, *ChemPhysChem* **2010**, *11*, 3231-3235.
[13] G. Ertl, *Science* **1991**, *254*, 1750-1755.
[14] C. Spiel, D. Vogel, Y. Suchorski, W. Drachsel, R. Schlögl, G. Rupprechter, *Catal. Lett.* **2011**, *141*, 625-632.
[15] D. Vogel, C. Spiel, Y. Suchorski, A. Urich, R. Schlögl, G. Rupprechter, *Surf. Sci.* **2011**, *605*, 1999-2005.

Entry for the Table of Contents

Heterogeneous catalysis

D. Vogel, C. Spiel, Y. Suchorski,
A. Trinchero, R. Schlögl, H. Grönbeck,
G. Rupprechter*

_____ Page – Page

Local light-off in catalytic CO oxidation on low-index Pt and Pd surfaces: a combined PEEM, MS and DFT study

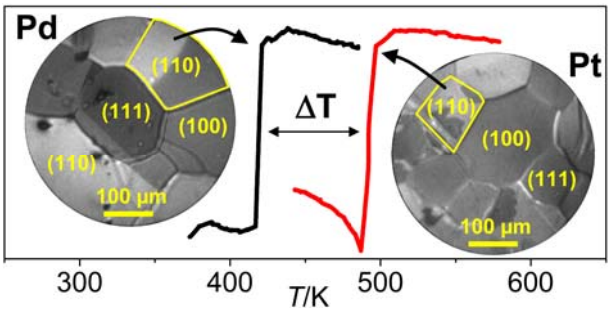

Shedding light on light-off: Photoemission electron microscopy, mass spectrometry, density functional theory and micro-kinetic modelling were employed to examine the local kinetics in the CO oxidation on individual grains of a polycrystalline sample. It is demonstrated that catalytic ignition occurs easier on Pd(hkl) domains than on corresponding Pt(hkl) domains. The isothermal determination of kinetic transitions, commonly used in surface science under high-vacuum conditions, is fully consistent with the isobaric reactivity monitoring usually applied in technical catalysis.

Supporting Information

S1. Global ignition/extinction measurements for Pt foil were performed by mass spectrometric monitoring of the CO_2 reaction rate at constant p_{O2} = 1.3x10^{-5} mbar and p_{CO} = 6.6 x10^{-6} mbar, as illustrated in Figure S1a. The global extinction curve appears to be smoothened out and a distinct "global extinction temperature" can hardly be assigned. This "smoothing" effect is caused by sequential extinction of differently oriented Pt(hkl) domains, i.e. at isobaric conditions the local extinctions on the individual Pt(hkl) domains occur sequentially within a broad temperature range which covers almost the whole global hysteresis loop. For comparison, a global R_{CO2} hysteresis curve obtained under isothermal conditions upon cyclic variation of the CO partial pressure is shown in Figure S1b. The smooth appearance of the transition τ_A upon CO pressure variation reflects again the sequential CO-poisoning of the (hkl) domains.

Parallel to the global MS measurements shown in Figures S1a and b, the local PEEM intensities from individual grains of the Pt foil were monitored, as shown in Figure S1c and d for a (100) domain. For both type of measurements, variation of temperature (Figure S1c) and variation of CO partial pressure (Figure S1d), the local kinetic transition points τ_A*/τ_B* and τ_A/τ_B, respectively, are much more pronounced than in the global MS measurements (Figures S1a, b).

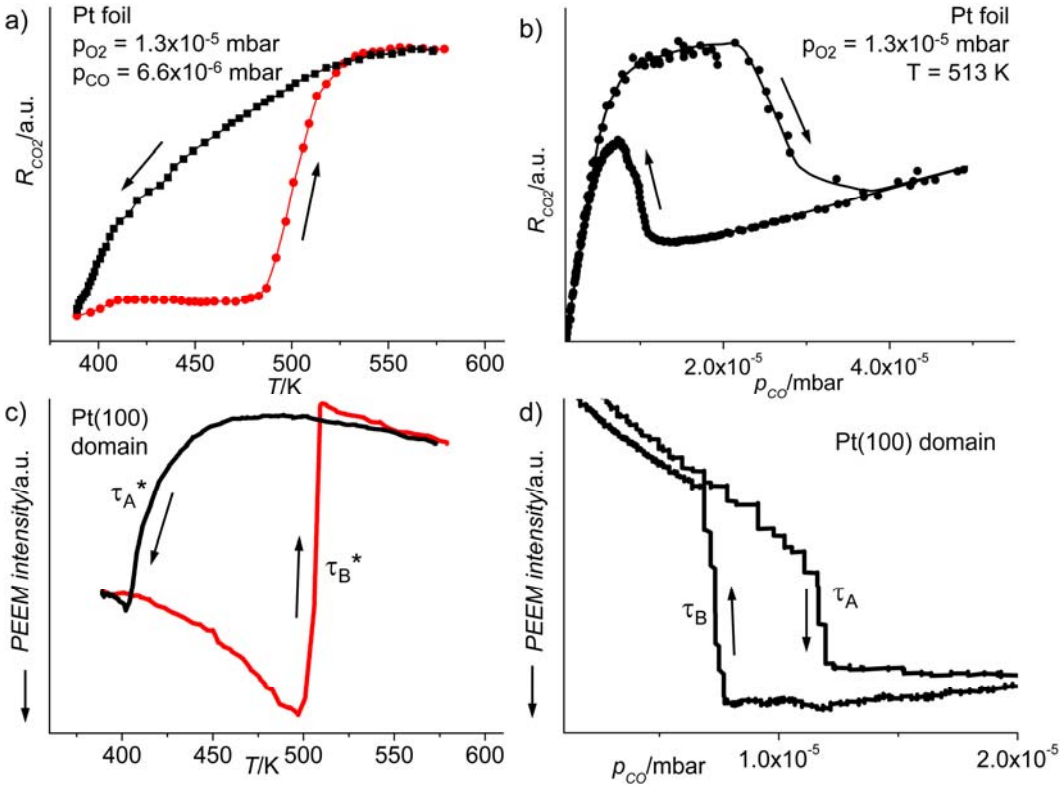

Figure S1. a) Global ignition (red) and extinction (black) R_{CO2} curves obtained for Pt foil upon cyclic temperature variation at constant p_{CO} = 6.6x10^{-6} mbar and p_{O2} = 1.3x10^{-6} mbar; b) global hysteresis in the CO_2 rate upon p_{CO} variation at T = 513 K, at the same oxygen pressure as in a); c) local PEEM intensity during ignition/extinction on a Pt(100) domain, simultaneously obtained with the R_{CO2} curve in a); d) local PEEM intensity hysteresis on a Pt(100) domain during CO pressure variation as shown in b).

S2. To obtain local ignition/extinction of Pt(hkl) domains, PEEM video-sequences were recorded simultaneously to the MS-monitoring, under isobaric reaction conditions (p_{CO} = 6.6x10^{-6} mbar and p_{O2} = 1.3x10^{-5} mbar). Details of the identification of the surface orientation of the individual Pt(hkl) domains and the contrast mechanism (CO-covered surface appears bright in

comparison to oxygen covered surface) were described in Ref. [S1]. Note that on Pt, contrary to Pd, the oxygen covered surface appears darker in PEEM than CO covered regions.

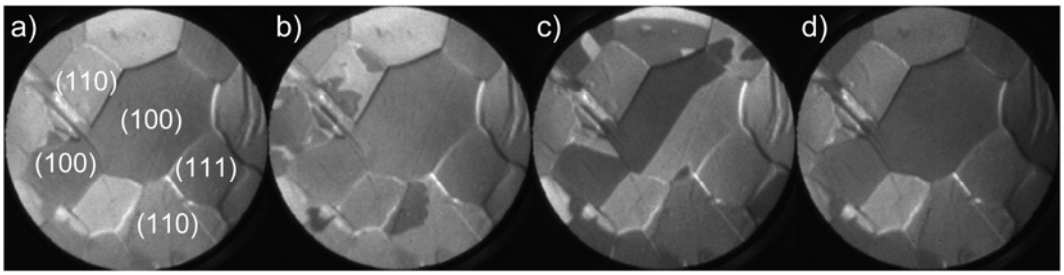

Figure S2. Sequence of PEEM images during the ignition τ_B* on Pt foil at constant p_{CO} = 6.6x10^{-6} mbar and p_{O2} = 1.3x10^{-5} mbar. The temperature is ramped with a heating rate of ~0.5 K/s from 483 K in frame (a) (CO-covered), to 492 K and 506 K in frame (b) and (c) (ignition on (110) and (100) domains) and to 568 K in frame (d) (oxygen covered). The orientation of the individual domains is indicated in frame a).

S3. Density Functional Theory Calculations

Density functional theory (DFT) was used in a real space grid implementation[S2, S3] of the projector augmented wave (PAW) method[S4] with a grid spacing of 0.18 Å. The frozen core and projectors were generated with scalar relativistic corrections for Pd and Pt. Exchange and correlation contributions were described by the spin-polarized Perdew-Burke-Ernzerhof (PBE) functional.[S5] Reciprocal space integration over the Brillouin zone was approximated with finite sampling.[S6, S7] An effective temperature of 0.1 eV was used to smear the Fermi discontinuity. Activation energies were evaluated with the nudged-elastic band method[S8] or constrained optimization.

Three surfaces were considered for Pd and Pt, namely (111), (100) and the missing row reconstructed (110). Four atomic layers were used to model the slabs. The calculations were performed with an adsorption coverage of 0.25. The structural relaxations were performed within the quasi-Newton method. Structures are regarded optimized when the largest element of the gradient was smaller than 0.05 eV/Å.

The energetic results from the DFT are collected in Table S1. Only adsorption of atomic oxygen was considered. Thus, the $E_{ads}(O_2)$ value in Table S1 corresponds to the adsorption energy of two oxygen atoms with respect to O_2 in the gas phase. The results are in good agreement with previous reports. It should be noted that the reaction barrier is sensitive to the assumed reaction path. For the (111) surfaces, the barrier is obtained from CO close to an atop position and O in a bridge configuration. CO_2 is in this case formed over an fcc hollow site. Over the (100) surfaces, CO_2 is formed from both CO and O in opposite bridge positions. On (110), the barrier is evaluated with CO in a bridge position on the row and O in a hollow position.

Table S1: Adsorption energies of CO and O_2 and the barrier (E_r) to form CO_2 from adsorbed CO and O on the three low Miller index planes of Pt and Pd, as well as the sticking coefficients of CO and oxygen and the desorption temperature of CO, as known from literature. The energies are reported in eV. The sticking coefficients used in the simulations are given in parentheses. The preferred adsorption sites are indicated for CO and O; atop (t), bridge (b), hollow (h) and fcc hollow (fcc).

	E_{ads}(CO)	E_{ads}(O_2)	E_r	s_0(O_2)	s_0(CO)	T_{des}(CO) [K]
Pt(110)	2.00 (t)	2.40 (h)	0.96	0.3-0.4[S9] (0.4)	0.8-1[S10] (0.9)	500-520[S10]
Pt(100)	2.02 (b)	2.14 (b)	0.55	10^{-3}/0.1[S11] (0.1)	0.6-0.75[S12] (0.6)	~520[S13]
Pt(111)	1.76 (fcc)	2.28 (fcc)	0.95	0.06[S14] (0.1)	0.6-0.8[S15] (0.9)	400-450[S16]
Pd(110)	1.97 (h)	2.48 (h)	-	0.96[S17]	1[S18]	400/475[S19]
Pd(100)	1.84 (b)	2.40 (h)	0.80	0.1-0.75[S20, S21]	0.6-0.8[S22]	~480[S22]
Pd(111)	1.96 (fcc)	2.50 (fcc)	1.53	0.7[S23] (0.7)	0.96[S24] (0.7)	450[S25]

S4. Micro-Kinetic Model

The micro-kinetic model is based on the conventional Langmuir-Hinshelwood mechanism for CO oxidation:

$CO + * \leftrightarrow CO*$ (R1)
$O_2 + 2* \leftrightarrow 2O*$ (R2)
$O* + CO* \leftrightarrow CO_2 + 2*$ (R3)

Here, * denotes a free surface site and X* an adsorbate X bonded to a surface site. The corresponding rate equations are:

$$\frac{d\theta_{CO}}{dt} = s_{CO}^0 (1-\theta_{CO}^2) p_{CO} k_{CO}^a - k_{CO}^d \theta_{CO} - k^r \theta_{CO} \theta_O$$

$$\frac{d\theta_O}{dt} = 2s_O^0 (1-\theta_{CO}-\theta_O)^2 p_{O_2} k_{O_2}^a - k_{O_2}^d \theta_O^2 - k^r \theta_{CO} \theta_O$$

Here, θ_{CO} and θ_O are the coverages, p_{CO} and p_{O_2} are the pressures, and s_{CO}^0 and $s_{O_2}^0$ the initial sticking coefficients. The rate constants are given by:

$$k_{CO}^d = \nu_{CO}^d e^{-E_{CO}^d (1-\alpha\theta_{CO})/k_B T}$$

$$k_{O_2}^d = \nu_{O_2}^d e^{-E_{O_2}^d (1-\alpha\theta_O)/k_B T}$$

$$k^r = \nu^r e^{-E^r (1-\beta\theta_{CO})/k_B T}$$

$$k_X^a = 1/N_0 \sqrt{2\pi M k_B T}$$

T is the temperature, k_B is the Boltzmann constant, M is the mass of the molecule under consideration, and N_0 is the number of sites per area. A linear coverage dependence is introduced for the adsorption energies and the barrier. α and β are in all cases set close to 0.5. The coverage dependence (strength and functional form) could, in principle, be evaluated from first principles. However, here we have followed the strategy in Ref. [S26]. The desorption of O_2 is included above for completeness. The kinetics is insensitive to this step and it was not included in the simulations. The pre-exponential factors are set to $\nu_{CO}^d = 10^{15}$ and $\nu^r = 10^{14}$, respectively [S26].

References

[S1] Y. Suchorski, C. Spiel, D. Vogel, W. Drachsel, R. Schlögl, G. Rupprechter, *ChemPhysChem* **2010**, *11*, 3231-3235.

[S2] J. J. Mortensen, L. B. Hansen, K. W. Jacobsen, *Phys. Rev. B* **2005**, *71*, 035109.

[S3] https://wiki.fysik.dtu.dk/gpaw.

[S4] P. E. Blöchl *Phys. Rev. B* **1994**, *50*, 17953-17979.

[S5] J. P. Perdew, K. Burke, M. Ernzerhof, *Phys. Rev. Lett.* **1996**, *77*, 3865-3868.

[S6] H. J. Monkhorst, J. D. Pack, *Phys. Rev. B* **1976**, *13*, 5188-5192.

[S7] J. D. Pack, H. J. Monkhorst, *Phys. Rev. B* **1977**, *16*, 1748-1749.

[S8] G. Henkelman, B. P. Uberuaga, H. J. Jónsson, *J. Chem. Phys.* **2000**, *113*, 9901-9904.

[S9] R. Ducros, R. Merrill, *Surf. Sci.* **1976**, *55*, 227-245.

[S10] R. McCabe, L. Schmidt, *Surf. Sci.* **1976**, *60*, 85-98.

[S11] P. Norton, K. Griffiths, P. Bindner, *Surf. Sci.* **1984**, 138, 125-147.

[S12] G. Brodén, G. Pirug, H. Bonzel, *Surf. Sci.* **1978**, *72*, 45-52.

[S13] R. J. Behm, P. A. Thiel, P. R. Norton, G. Ertl, *J. Chem. Phys.* **1983**, *78*, 7437-7447.

[S14] Y. Y. Yeo, L. Vattuone, D. A. King, *J. Chem. Phys.* **1997**, *106*, 392-401.

[S15] C. T. Campbell, G. Ertl, H. Kuipers, J. Segner, *Surf. Sci.* **1981**, *107*, 207-219.

[S16] G. Ertl, M. Neumann, K. M. Streit, *Surf. Sci.* **1977**, *64*, 393-410.

[S17] K. Yagi, D. Sekiba, H. Fukutani, *Surf. Sci.* **1999**, *442*, 307-317.

[S18] J. Goschnick, M. Grunze, J. Loboda-Cackovic, J. H. Block, *Surf. Sci.* **1987**, *189-190*, 137-146.

[S19] J. Goschnick, M. Wolf, M. Grunze, W. N. Unertl, J. H. Block, J. Loboda-Cackovic, *Surf. Sci.* **1986**, *178*, 831-841.

[S20] T. Orent, S. Bader, *Surf. Sci.* **1982**, *115*, 323-334.

[S21] A. Gerbi, L. Savio, L. Vattuone, F. Pirani, D. Cappelletti, M. Rocca, *Angew. Chem.* **2006**, *118*, 6807-6810; *Angew. Chem. Int. Ed.* **2006**, *45*, 6655-6658.

[S22] R. J. Behm, K. Christmann, G. Ertl, M. A. van Hove, *J. Chem. Phys.* **1980**, *73*, 2984-2995.

[S23] F. P. Leisenberger, G. Koller, M. Sock, S. Surnev, M. G. Ramsey, F. P. Netzer, B. Klötzer, K. Hayek, *Surf. Sci.* **2000**, *445*, 380-393.

[S24] T. Engel, *J. Chem. Phys.* **1978**, *69*, 373-385.

[S25] X. Guo, J. T. Yates, *J. Chem. Phys.* **1989**, *90*, 6761-6766.

[S26] P.-A. Carlsson, M. Skoglundh, P. Thormählen and B. Andersson, *Top. Catal.* 2004, *30/31*, 375-381.